SIMULATION ANALYSIS AND EXPERIMENTAL STUDY ON THE IMPROVED STRUCTURAL DESIGN OF A CROSS-FLOW RICE DRYING SECTION BASED ON EDEM–FLUENT COUPLING

/

基于 EDEM-Fluent 的稻谷横流干燥段结构改进设计的仿真分析与试验

Hao-chen WANG[1)], Gang CHE[*1,2)], Lin WAN[1,2)], Shu-guo HE[3)], Zheng-fa CHEN[1)], Yan-qi YAN[1)]

[1)] College of Engineering, Heilongjiang Bayi Agricultural University, Daqing / P.R.China

[2)] Heilongjiang Agricultural Machinery Intelligent Equipment Key Laboratory, Daqing / P.R.China

[3)] Heilongjiang Academy of Agricultural Machinery Engineering Science Jiamusi Branch, Jiamusi / P.R.China

Tel: +86-459-13836961617; E-mail: chegang180@126.com

Corresponding author: Gang Che

DOI: https://doi.org/10.35633/inmateh-77-120

Keywords: *drying of rice; transverse flow; grain turning device; numerical simulation; test; CFD–DEM coupling*

ABSTRACT

To address the uneven drying issue caused by temperature gradients during the cross-flow drying of paddy, this study designs a grain-turning device that periodically rotates clockwise, based on the cross-flow ventilation drying process of paddy. The device is intended to promote sufficient mixing of paddy grains in the drying section, thereby enhancing the drying uniformity and processing quality of paddy. Based on the thermo-hydro-mechanical (THM) coupling theory, computational fluid dynamics (CFD), and discrete element method (DEM) for particles, two mathematical analytical models of the cross-flow drying section (with and without the grain-turning device) were established. Using the EDEM-Fluent software coupling method, numerical simulations were conducted to investigate the variation patterns of temperature and moisture content of paddy grains in the two drying sections. The results indicate that the drying section equipped with the grain-turning device can effectively resolve the uneven distribution of moisture content and temperature in the grain layer caused by the air supply direction, verifying the feasibility of the device. To further verify its performance, a comparative experiment was carried out under the same parameters (drying duration: 100 min): before the improvement, the average moisture content of paddy in each layer was 15.24%, with a standard deviation of 1.26 and a variance of 1.59; after the improvement, the average moisture content decreased to 14.61%, with a standard deviation of 0.192 and a variance of 0.037. One-way analysis of variance (ANOVA) shows that the inter-group F-statistic reaches 41.536, which is much higher than the critical value (4.41) corresponding to the significance level of 0.05, with $p < 0.001$.In conclusion, the drying uniformity of paddy with the grain-turning device is significantly superior to that of conventional drying, providing a practical technical reference for the optimization of paddy drying production processes.

摘要

针对稻谷横流干燥过程中因温度梯度引发的干燥不均匀问题，本文基于稻谷横流通风干燥工艺，设计一种可周期性顺时针运动的谷物翻粮装置，以促进干燥段内稻谷颗粒充分混合，进而提升稻谷干燥均匀性与加工品质。基于热流固耦合理论（THM）、计算流体动力学（CFD）与颗粒离散元法（DEM），建立了包含有无翻粮装置的两种横流干燥段数学解析模型，采用 EDEM-Fluent 软件耦合方法，对两种干燥段内稻谷颗粒的温度及含水率变化规律进行数值模拟。结果表明：配备翻粮装置的干燥段可有效解决因送风风向导致的粮层含水率与温度分布不均问题，验证了该装置的可行性。为进一步验证效能，在相同参数下（干燥时长 100 min）开展对比试验：改进前各层稻谷含水率均值 15.24%、标准差 1.26、方差 1.59；改进后均值降至 14.61%、标准差 0.192、方差 0.037。单因素方差分析显示，组间 F 统计量达 41.536，远高于显著性水平 0.05 对应的临界值（4.41），且 $p<0.001$。综上，配备翻粮装置的稻谷干燥均匀性显著优于常规干燥，为稻谷干燥生产工艺的优化提供了切实可行的技术参考。

Hao-chen Wang, master degree; Gang Che, Prof. Ph.D.; Lin Wan, Prof. Ph.D.; Shu-guo He, Ph.D.; Zheng-fa Chen, Ph.D.; Yan-qi Yan, master degree.

INTRODUCTION

Rice is one of the most crucial staple crops globally and occupies a core position in China's food security system. According to the 2024 Grain Production Bulletin issued by the National Bureau of Statistics, China's total paddy output reached 207.535 million tons (*Lv et al., 2010*). Freshly harvested paddy typically contains high moisture content; if the moisture level fails to be reduced to the safe storage range (14.0%–14.5%), accumulation of heat and moisture can readily induce mold growth and insect infestation, resulting in substantial post-harvest losses (*Xiao et al., 2025*). Therefore, optimizing rice drying processes and equipment is not only essential for reducing drying costs and ensuring grain quality, but also for increasing farmers' income and stabilizing the food supply chain (*Wu et al., 2011; Zhang et al., 2021; Xu et al., 2020*).

Based on the relative flow directions of the material and drying medium, hot-air drying is generally categorized into four modes: cross-flow, concurrent-flow, counter-flow, and mixed-flow (*Wu et al., 2001*). Among these, cross-flow dryers are the most widely used commercial grain dryers globally, attributed to their simple structure, low equipment cost, and convenient operation *(Schluterman et al., 2004)*. Nevertheless, cross-flow ventilation has an inherent limitation: hot air is supplied from only one side of the grain bed, leading to non-uniform drying. Paddy near the air inlet side tends to dry excessively rapidly, causing overheating and grain fissuring, while paddy on the leeward side often remains under-dried. This results in significant non-uniformity in moisture distribution, which severely restricts processing quality and drying efficiency. Although recent advancements have been achieved in structural optimization, numerical simulation, and theoretical research, cost-effective and easily implementable solutions to the core issue of cross-flow drying non-uniformity remain insufficient.

To address this challenge, researchers worldwide have explored various approaches. In terms of structural improvements, designs such as cross-flow deflectors, optimized heating tube arrangements, airflow guide plates, inclined baffles, and grain inverters have been proposed (*Prakash et al., 2018; Li et al., 1998*). While these methods can partially enhance drying uniformity, they are often plagued by poor compatibility with existing equipment and high retrofitting costs, limiting their applicability for small- and medium-sized enterprises. From the simulation perspective, computational fluid dynamics-discrete element method (CFD-DEM) coupled models have been employed to optimize the structures of hot-air chambers (*Yin et al., 2025*), whereas standalone CFD simulations have been utilized to analyze airflow characteristics, temperature-humidity distributions, and moisture migration behaviors within grain beds (*Kjær et al., 2018; Chen et al., 2014; Li et al., 2014*). Beyond these applications, CFD technology has also facilitated the design and simulation of dryers equipped with heat recovery capabilities, such as innovative vertical dryers and small-capacity pilot-scale drying units. Leveraging the heat recovery design of these devices enables the recovery of heat lost from the drying medium, thereby achieving a significant reduction in energy consumption. Additionally, CFD-based simulations support the structural optimization of key components (e.g., cylindrical chambers and deflector plates) and contribute to the attainment of uniform temperature distribution across the seed bed (*Carlescu et al., 2018; Arsenoaia et al., 2019*). However, these studies rarely integrate with practical structural innovations, reducing their direct engineering applicability. Theoretical research has also investigated moisture binding energy, energy consumption distribution, and exergy transfer characteristics during rice drying (*Li et al., 2014; Li et al., 2023*), providing insights into the energy mechanisms underlying moisture migration.

In summary, this study aims to achieve uniform drying of paddy within the drying section. Accordingly, a grain-turning device was designed. Using EDEM (based on the discrete element method, DEM) and Fluent (computational fluid dynamics, CFD), a coupled simulation model integrating paddy particles, interphase mass transfer, and the grain-turning mechanism was established. Comparative simulations were conducted for cross-flow drying sections with and without the proposed device, and experimental validation was performed. Furthermore, key drying process parameters were optimized to enhance drying efficiency, improve drying uniformity, and ultimately elevate rice processing quality.

Physical simulation model of cross-flow drying

Structural Design and Operating Principle of the Drying Section

Based on the concept of cross-flow drying process, the fundamental structure of the drying sectio n was constructed, and a three-dimensional model was developed. A schematic diagram of the operat ing principle is shown in Figure 1. Based on the principle of cross-flow drying technology, a cross-flo w drying section was designed with an inner diameter of 100 mm and a length of 100 mm. Driven b y a motor, the grain-turning device rotates clockwise inside the drying section. The agitation of rice gr ains by the device promotes thorough mixing of the inner and outer layers of the grain bed, thereby

achieving the goal of uniform drying. For this purpose, the basic structure of the drying section was c onstructed, and a three-dimensional model was established. A schematic diagram of the working princ iple is shown in Fig. 1.

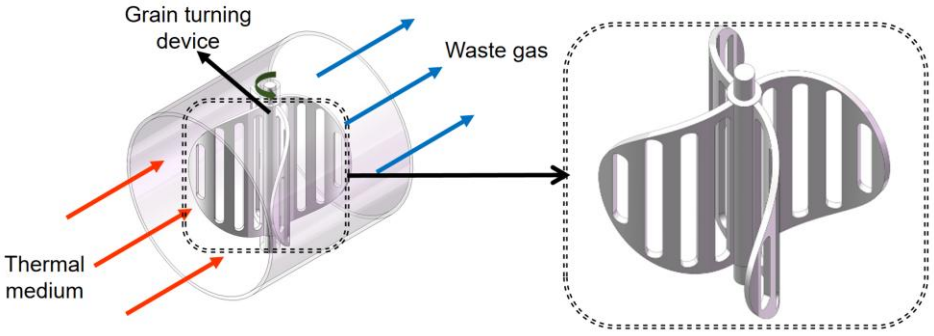

Fig. 1 - Structure diagram of drying section and grain turning device

As shown in Fig. 1, the grain-turning device has an outer diameter of 90 mm and a height of 90 mm, with its blades bent 90° along the transverse direction. To reduce the stress exerted on the device by rice grains during rotation and minimize the blocking effect of the device on transverse hot air flow within the drying section, straight-slotted grilles are opened on the blades. Each grille has a width of 5 mm and a spacing of 5 mm, which can increase the transverse hot air circulation area. By cooperating with the periodic disturbance of the particle layer by the helical blades, the device not only expands the transverse air exposure area of rice grains but also reduces the plastic deformation stress acting on rice kernels during the device's rotation, thereby extending the service life of the grain-turning device.

Mathematical model

The fluid–solid coupling domain consists of both the fluid and solid regions. In the rice drying process, the hot-air medium can be regarded as a continuous phase, while the dried rice grains are discretely distributed within the medium. To facilitate the modeling and analysis of the drying process, the following assumptions are made: (1) The shrinkage of rice grains during drying is neglected. (2) Heat and mass transfer between rice grains and the gas phase occurs only through convection. (3) Moisture migration inside the rice kernels occurs exclusively in the liquid phase, and evaporation takes place solely at the particle surface. (4)The latent heat required for moisture evaporation at the surface is entirely supplied by the rice grain itself *(Li et al., 2023)*.

Particle Governing Model

The contact forces acting on a particle, expressed in Equations (1–3), consist of normal and tangential components:

$$F_{\mathrm{n}} = k_n \delta_n - \eta_n \nu_{r,n} \tag{1}$$

$$F_t = -\mu_{\mathrm{f}} F_n \frac{\nu_{r,t}}{|\nu_{r,t}|} \quad |F_t| > \mu_{\mathrm{f}} |F_n| \tag{2}$$

$$F_t = -k_t \delta_t - \eta_t \nu_{r,t} \quad |F_t| \,,, \mu_{\mathrm{f}} |F_n| \tag{3}$$

where: k is the elastic modulus, [N·m⁻¹]; δ is the inter-particle deformation, [m]; η is the damping coefficient, [N·m⁻¹·s]; ν_{r} is the relative velocity between particles, [m·s⁻¹]; μ_{f} is the sliding friction coefficient; subscripts n and t represent the normal direction and tangential direction, respectively.

Based on the solid phase assumption, the heat and mass transfer conservation equation inside the rice is:

$$\rho_s C_{ps} \frac{\partial T}{\partial t} = \nabla(\kappa \cdot \nabla T) + Q_{eva} \tag{4}$$

where: ρ_s is the average density of the solid phase, [kg/m³]; C_{ps} is the specific heat capacity at constant pressure, [J/(kg·K)]; κ is the thermal conductivity inside the solid phase, which varies with the moisture content inside the particles, [J/(m·s·K)]; T is the temperature of the solid phase, [K]; Q_{eva} is the latent heat of moisture evaporation, [J/(m³·s)].

$$\frac{\partial M}{\partial t} = \nabla(D_{eff} \cdot \nabla M) \tag{5}$$

where: M refers to the moisture mass concentration inside rice particles (i.e., mass of moisture per unit volume of particles), [kg/m^3]; D_{eff} is the effective moisture diffusion coefficient inside particles, [m²/s].

Gas phase control model

The model assumes that the rice layer is a uniform porous medium. The key to describing air flow is to quantify its drag in the valley, which is achieved by introducing a momentum source term S_i into the momentum conservation equation. The momentum conservation equation is expressed as follows:

$$\frac{\partial \vec{u}}{\partial t} + (\vec{u} \cdot \nabla)\vec{u} = -\frac{1}{\rho_a}\nabla p + \frac{\mu}{\rho_a}\nabla^2 \vec{u} + S_i \tag{6}$$

The momentum source term S_i includes two parts: one is the loss caused by viscous resistance, and the other is the loss caused by inertial resistance. The simplified momentum source term S_i can be expressed as:

$$S_i = -\left(\frac{\mu}{\alpha} v_j + C_2 \frac{\rho_a}{2} |v| v_j\right) \tag{7}$$

where: μ is the dynamic viscosity of the fluid, [Pa·s]; p for pressure, [Pa]; $|v|$ is the speed scalar size, [m/s]; v_j is the velocity component of three-dimensional space, [m/s]; 1/ α is the viscous resistance coefficient, [m^{-2}]; C_2 is the inertial resistance coefficient (dimensionless).

The corresponding component transport equation and energy conservation equation are as follows:

$$\frac{\partial}{\partial t}(\rho_g Y_i) + \nabla \cdot (\rho_g U Y_i) = \nabla \cdot (\rho_g D_{eff} \nabla Y_i) \tag{8}$$

$$\frac{\partial}{\partial t}(\rho_g U h) + \nabla \cdot (\rho_g U h) + \frac{\partial}{\partial t}(\rho_g K_e) + \nabla \cdot (\rho_g U K_e) - \frac{\partial p}{\partial t} = \nabla \cdot (\alpha_{eff} \nabla h) \tag{9}$$

For the above parameters, ρ_g , p, and h are the density [kg/m^3], pressure (Pa), and apparent enthalpy of the gas phase mixture, respectively, U is the velocity [m/s], g is the local gravitational acceleration [m²/s], and Y_i represents the mass fraction of each component in the gas phase mixture. In the energy equation 9, K_e is the kinetic energy of the gas phase mixture, and α_{eff} represents K/Cp (the ratio of thermal conductivity to specific heat capacity). D_{eff} is called the equivalent thermal diffusion coefficient, and can also be regarded as the equivalent mass diffusion coefficient.

Simulation model and parameter settings

Particle Model

In this study, the DEM numerical simulation is based on the rice variety “Daohuaxiang 2,” produced by the Wuchang Rice Factory of Beidahuang Group. A total of 1,000 rice kernels were randomly selected for dimensional measurement, yielding the following average tri-axial dimensions: length 7.76 mm, width 1.78 mm, and thickness 2.53 mm. A single particle model corresponding to this rice variety was used throughout the simulation. Considering the relatively regular morphology of rice grains, a particle geometry composed of 11 spheres with different radii was constructed. The geometric configuration of the model in EDEM is illustrated in Fig. 2.

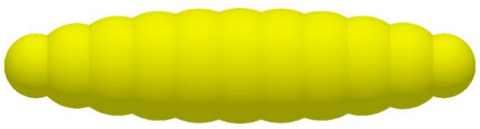

Fig. 2 - Rice Particle Model

Parameter Settings

The operational conditions of the drying section were simulated using the EDEM–Fluent coupled heat-transfer method. The physical parameters of rice grains and stainless steel are listed in Table 1 *(Jia et al., 2014; Wan et al., 2019; Sweet et al., 1987; Yang et al., 2003)*. The Hertz–Mindlin (no-slip) model *(Hou et al., 2018)* was selected as the contact model, and the initial temperature of the rice particles was set to 17°C. The DEM contact parameters between rice grains and stainless steel were defined in the EDEM Particle Factory. Since the exhaust outlet of the drying section is directly connected to the ambient environment, its boundary condition was specified as a gauge pressure of 0 Pa.

Table 1

The relevant simulation parameters used in this paper

Parameter	Value
Poisson's ratio of rice	0.25
Elastic modulus of rice/MPa	375
Actual density of rice grains/(kg·m^{-3})	1350
Thermal conductivity of rice grains/(W·(m·K)$^{-1}$)	0.1
Thermal diffusivity of rice grains/(m^2·s^{-1})	1.2
Specific heat capacity of rice/(kJ·(kg·K)$^{-1}$)	1.5
Poisson's ratio of stainless steel	0.29
Elastic modulus of stainless steel/MPa	75000
Density of stainless steel/(kg·m^{-3})	8000
Thermal conductivity of stainless steel/(W·(m·K)$^{-1}$)	16.2
Thermal diffusivity of stainless steel/(m^2·s^{-1})	4.4·10^{-6}
Specific heat capacity of stainless steel/(kJ·(kg·K)$^{-1}$)	0.49
Coefficient of restitution (rice-rice)	0.6
Coefficient of restitution (rice-stainless steel)	0.5
Static friction coefficient (rice-rice)	0.3
Static friction coefficient (rice-stainless steel)	0.56
Dynamic friction coefficient (rice-rice)	0.01
Dynamic friction coefficient (rice-stainless steel)	0.02
Air density/(kg·m^{-3})	1.15
Thermal conductivity of air/(W·(m·K)$^{-1}$)	0.026
Specific heat capacity of air/(kJ·(kg·K)$^{-1}$)	1.005
Dynamic viscosity of air/(Pa·s)	1.6·10^{-5}
Convective heat transfer coefficient of air/(W·(m·K)$^{-1}$)	20

Based on the discrete element parameters specified in the table, these values were input into the EDEM particle factory to calculate the mass of a single rice particle, followed by the generation of 15,000 particle models. Subsequently, the generated particle system was imported into Fluent via the coupling interface. Under standard atmospheric pressure, the boundary conditions for the inlet and outlet of the drying section were configured as a velocity inlet and a pressure outlet, respectively, with the hot-air temperature set to 50 °C. Reynolds number (Re) calculations yielded a value greater than 2000, confirming that the fluid flow within the drying section exhibits turbulent characteristics. For numerical simulations, the k-ε turbulence model was selected first, as it is widely recognized for its reliability in simulating fully developed turbulent flows with Re > 1000–2000—consistent with the calculated Re range in this study—and its suitability for gas-solid flow scenarios in confined spaces *(Duraisamy et al., 2019)*. Subsequently, the Eulerian multiphase flow model was applied to resolve the gas-solid coupling process *(Padding et al., 2015; Ariyaratne et al., 2016)*.

SIMULATION RESULTS AND ANALYSIS

Analysis of Temperature Uniformity of Rice Particles

Two drying sections were simulated under identical operating conditions: the inlet airflow velocity was set to 2 m/s, the hot-air temperature was maintained at 55°C, and a total of 15,000 rice particle models were established. The grain-turning device was programmed to rotate 180° at 15-s intervals, with each rotation cycle lasting 2 s.

To better visualize the influence of the grain-turning device on rice particles, Ensight post-processing software was employed to color-code particles with temperatures ranging from 17°C to 19°C. During the first rotation cycle of the grain-turning device (15–18 s), the temperature and flow characteristics of rice particles in both drying sections were monitored. The temperature distribution of the rice particles under this condition is presented in Figure 3.

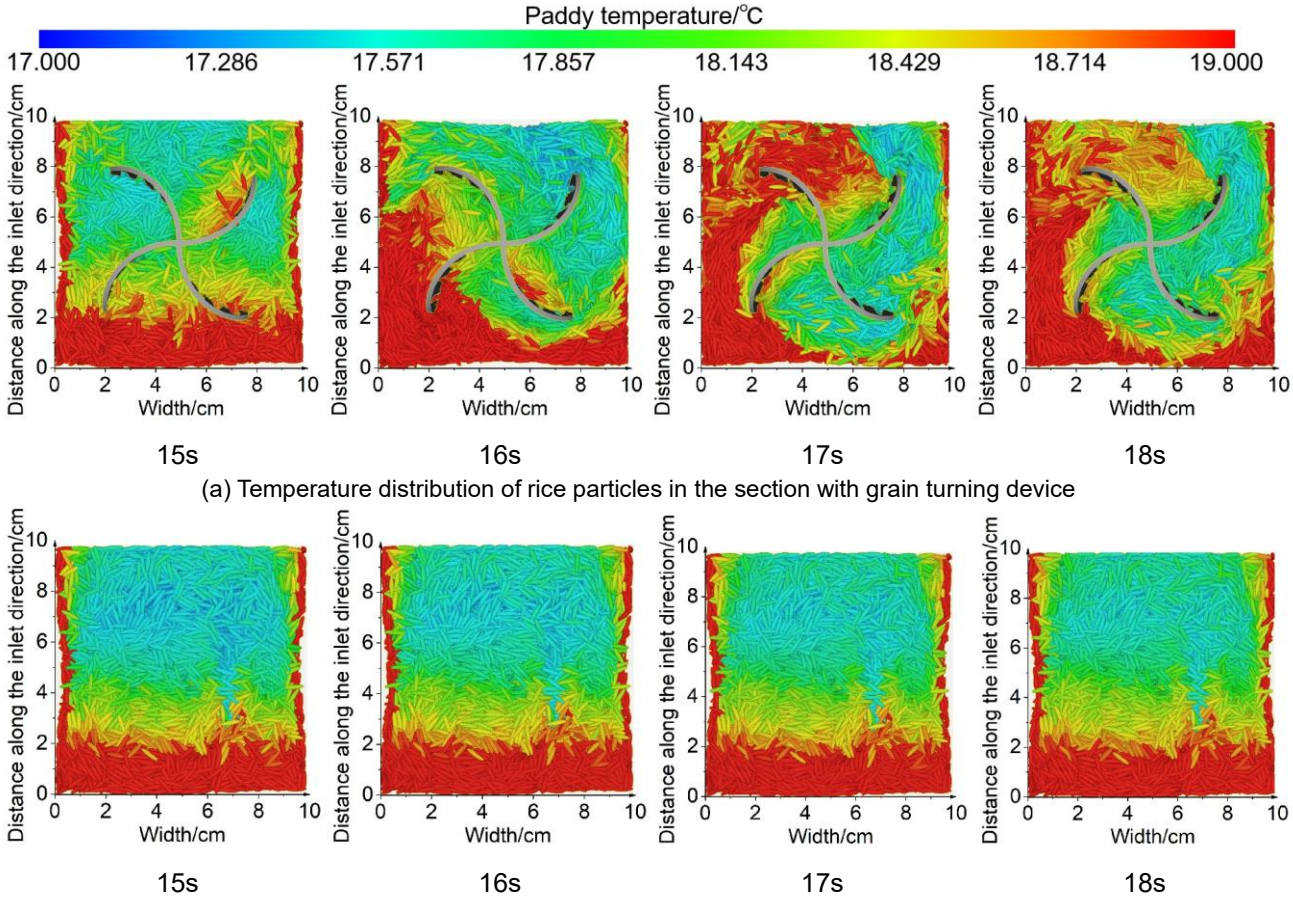

(a) Temperature distribution of rice particles in the section with grain turning device

(b) The temperature distribution of rice particles in the section without grain turning device

Fig. 3 - Temperature distribution of rice particles in two drying sections

As illustrated in Fig.3, for the drying section equipped with the grain-turning device, the following temperature and particle movement characteristics were observed: at t = 15 s, the temperature of rice particles near the air-inlet side and adjacent to the inner wall increased significantly. At t = 16 s, the grain-turning device rotated 90° clockwise over a 1-s period; this rotation drove the high-temperature rice particles near the air inlet to migrate toward the left side of the drying section, while the low-temperature rice particles near the outlet side moved toward the right side. At t = 17 s, the device rotated a further 90° clockwise within another 1-s period and then stopped, with the next rotation scheduled to occur after a 15-s interval. During this second rotation phase, the high-temperature rice particles on the left side of the drying section shifted toward the outlet side, whereas the low-temperature rice particles on the right side migrated toward the air-inlet side. By t = 18 s, the temperature of rice particles near the outlet side had decreased noticeably, by approximately 0.3 °C, while the temperature of particles near the air-inlet side increased by roughly 0.4 °C; no significant temperature fluctuations were detected in other regions.

In contrast, for the drying section without the grain-turning device, the temperature of rice particles remained largely stable during the 15–18 s period. Rice particles near the air-inlet side and adjacent to the inner wall maintained relatively high temperatures: a high-temperature zone was identified within 2 cm from the air inlet along the airflow direction, while the temperature of rice particles gradually decreased in the 2–10 cm range.

Analysis of Moisture Content Uniformity of Rice Particles

Both drying sections were further analyzed under identical operating conditions: hot-air temperature of 50 °C, airflow velocity of 2 m/s, initial moisture content of 25%, and a total of 15,000 rice particles. To more intuitively demonstrate the effect of the grain-turning device on rice particles, the device was set to rotate 180° clockwise at 5-s intervals, with each rotation lasting 2 s. The moisture content distributions of rice particles at 10 s, 20 s, 30 s, and 40 s were color-coded respectively, and the corresponding moisture content distribution of rice particles is presented in Fig. 4.

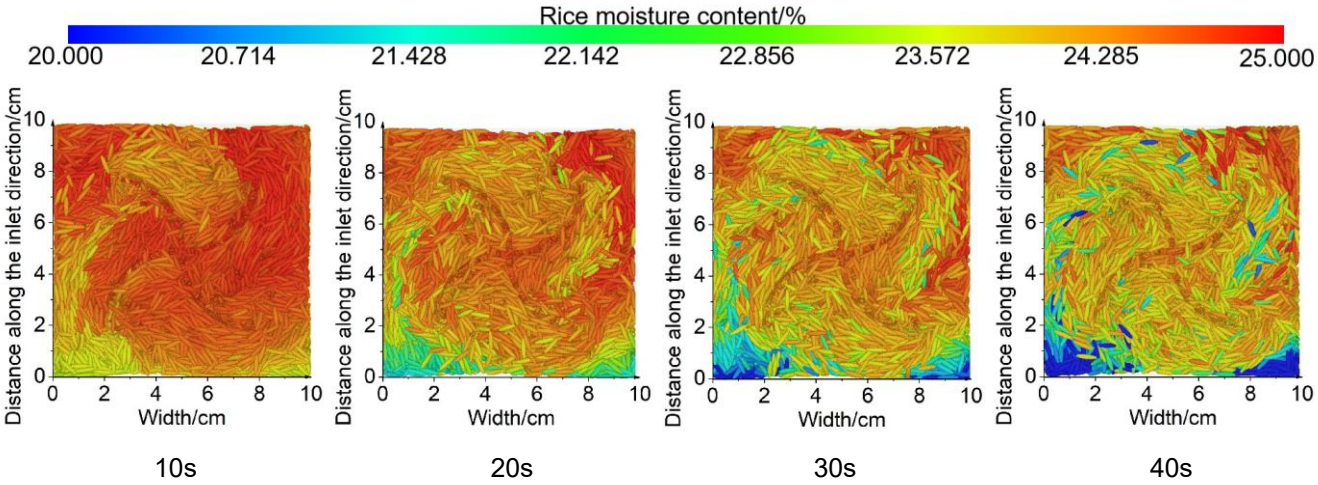

(a) Distribution map of moisture content of rice particles in the section with grain turning device

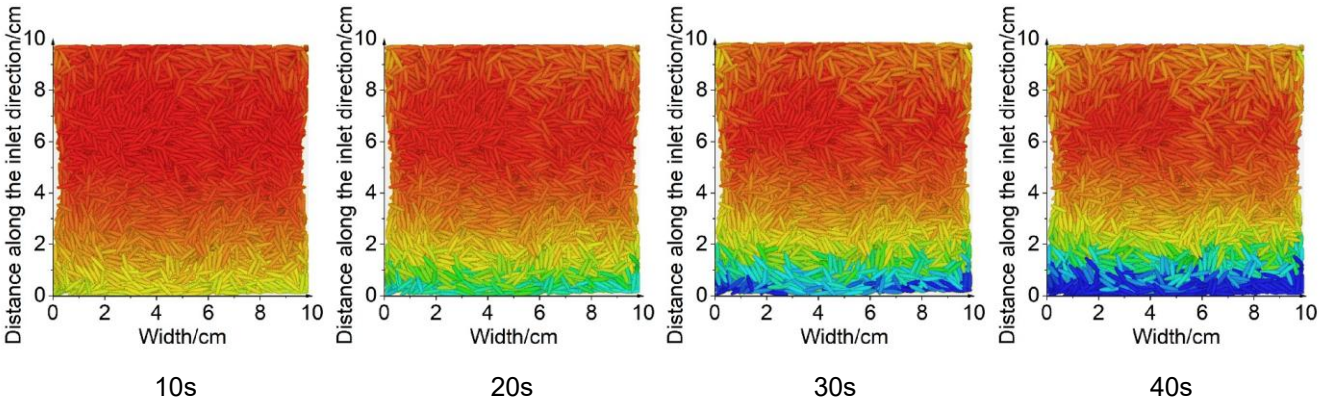

(b) Distribution map of moisture content of rice particles in no-turning device section

Fig. 4 - Distribution of moisture content of rice particles in two drying sections

Fig. 4 illustrates the moisture content distribution of rice particles along the vertical (gravity) direction in both drying sections (with and without the grain-turning device) over the 40-s drying period. At 10 s of drying, the section equipped with the grain-turning device had completed one periodic rotation, during which the low-moisture rice particles near the air-inlet side migrated toward the outlet side. At 20 s, rice particles with different moisture contents were thoroughly mixed within the section under the device's rotation, though the rice particles near the hot-air inlet exhibited excessive drying rates. At 30 s, the overall moisture content of rice particles decreased significantly, and sufficient particle mixing resulted in good drying uniformity. By 40 s, the mixing degree showed no significant change compared to that at 30 s, while the overall drying effect continued to improve.

In contrast, in the drying section without the grain-turning device, the moisture content of rice particles exhibited a distinct gradient along the airflow direction during the 10–40 s drying period. Rice particles near the air-inlet side underwent a marked reduction in moisture, whereas those near the outlet side (leeward side) showed minimal drying effects. This uneven drying may cause overheating and kernel fissuring on the windward side, ultimately leading to non-uniform drying. Although the overall drying rates of the two sections were comparable, the section equipped with the grain-turning device achieved significantly better drying uniformity due to thorough particle mixing.

RICE DRYING TEST

Materials and Equipment

The rice variety “Daohuaxiang 2” from the Wuchang Rice Factory of Beidahuang Group was selected as the experimental material, with a wet-basis moisture content of 23.8%–24.6%. The experiments were conducted in the Intelligent Drying Equipment Laboratory at Heilongjiang Bayi Agricultural University, using a self-developed physical model of a cross-flow drying test bench, as shown in Fig. 5.

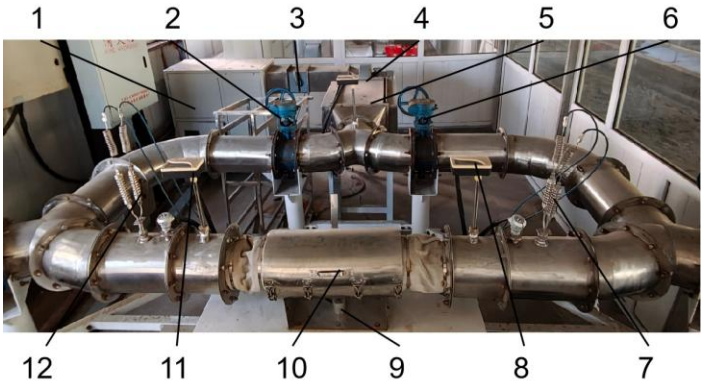

Fig. 5 - Cross-flow drying test bench

1-Constant temperature and humidity box; 2-Valve a; 3-Manual air regulating valve; 4-Fan; 5-Heater; 6-Valve b; 7-Wind speed sensor a; 8-Temperature and humidity sensor a; 9-Weighing sensor; 10-Drying room; 11-Temperature and humidity sensor b;12-Wind speed sensor b

As shown in Fig. 5, the test bench primarily consists of an intelligent control cabinet, a fan, a heater, a constant temperature and humidity chamber, and a drying chamber. During drying, the hot airflow generated by the constant temperature and humidity chamber is conveyed through the fan and heater into the drying chamber under the regulation of the control cabinet, completing the circulation of the drying air. The grain-turning device is integrated within and acts inside the drying chamber. The drying chamber is a cylindrical stainless-steel welded structure with a diameter of 100 mm. Two removable stainless-steel mesh screens are installed inside the cylinder to accommodate material samples of different thicknesses. The test bench employs a horizontal air supply method, effectively eliminating wind pressure in the vertical direction and reducing errors in vertical weight measurements of the material. Multiple valve combinations allow for adjustment of hot-air flow direction by switching valve states. Weight sensors collect signals reflecting changes in the mass of material within the drying chamber, enabling real-time monitoring of moisture loss. Temperature and airflow sensors transmit data to the processing system for real-time monitoring of pipeline temperature and airflow parameters. After drying, a custom-built rice fissure lamp is used to observe kernel cracking.

Simulation model and grid independence verification

In computational fluid dynamics (CFD) and other numerical simulations, grid independence verification is a critical step to ensure the accuracy and reliability of results, as the grid density has a decisive impact on computational precision. All simulations in this study were performed on a platform equipped with an AMD Ryzen 7 7840H CPU and an NVIDIA GeForce RTX 4060 GPU (GPU acceleration enabled). During the simulation, overly coarse grids may fail to capture flow-field details or gradients of physical quantities, whereas excessively refined grids significantly increase computational cost and simulation time, thereby reducing efficiency.

Transient simulations were conducted for 60 s under the set parameters. At 40 s, the temperature and moisture content of rice particles approached a stable trend, and therefore, the conditions within the 40 s window were the focus of this study.

The numerical simulation integrated the discrete element method (DEM) coupling and interphase mass transfer modules. Model validation was implemented under specific parameters: initial moisture content of 25% (wet basis), hot-air temperature of 50 °C, and inlet airflow velocity of 2 m/s. A cross-flow rice drying experiment was conducted under identical conditions, where temperature sensors and weighing sensors were employed to acquire experimental data. To ensure validation accuracy, the filling ratio of rice particles and external environmental conditions were kept consistent with those in the simulation. The results of the mathematical model and grid independence verification at 40 s are presented in Fig. 6.

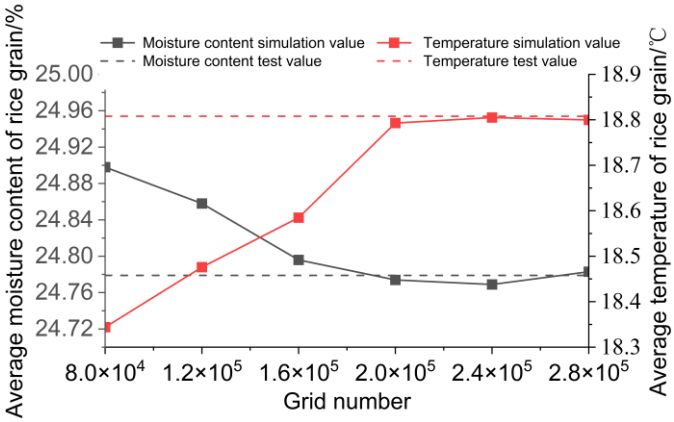

Fig. 6 - Establishment of the numerical model and analysis of grid independence verification

As illustrated in Fig. 6, when the grid number was below 2×10^6, the simulation values were significantly lower than the experimental values and failed to meet the simulation accuracy requirements. When the grid number reached 2×10^6, the numerical simulation results were in good agreement with the experimental values, with a relative error of 4.71% between them. With a further increase in grid number, no significant deviation was observed between the experimental and simulation values. Therefore, setting the grid number to 2×10^6 not only ensures simulation accuracy but also reduces computational cost.

Uniformity test of two rice drying methods

To verify the effect of the device (before and after modification) on rice drying uniformity, rice samples with identical physicochemical properties were selected in this study, and five parallel experiments were conducted under consistent operating conditions. The operating parameters of the drying section were kept uniform before and after modification—specifically, the operating interval of the built-in grain-turning device in the modified drying section was set to 15 s—and the total drying time for each group was 100 min.

After the completion of drying, the rice was completely removed from the drying section and evenly spread on a stainless steel plate, with strict preservation of their initial relative positions in the transverse direction. In accordance with the stratification scheme illustrated in Fig. 7, the rice was divided into 10 sampling layers. The moisture content of rice in each layer was measured using a Kett PM-8188New grain moisture meter (Shanghai Guanwei Instrument Co., Ltd., Shanghai, China). The average moisture content measured for each layer is presented in Table 2.

Fig. 7 - Distribution of rice sampling layer in the drying section

Table 2

Moisture Content and Parameters of Sampling Layer

Test scheme	1	2	3	4	5	6	7	8	9	10
Before improvement	13.4	13.9	14.2	14.6	14.9	15.3	15.8	16.3	16.8	17.2
Improved	14.5	14.7	14.2	14.8	14.5	14.7	14.6	14.9	14.7	14.5

As presented in Table 2, under identical drying process parameters for the two drying sections, the average moisture content of rice in each layer of the unmodified drying section (without a grain-turning device) was 15.24%, with a standard deviation of 1.26 and a variance of 1.59. For the modified drying section (equipped with a grain-turning device), the average moisture content of rice in each layer was 14.61%, accompanied by a standard deviation of 0.192 and a variance of 0.037. Specifically, the variance ratio (unmodified vs. modified) reached 43.03, and the standard deviation ratio was 6.57.

Experiment results and analysis

The variance analysis of the effects of different drying methods on the uniformity of rice moisture content was carried out. The results are shown in table 3 : Drying method as a factor between groups, the sum of squares is 3.9645, the degree of freedom is 1, the corresponding F value is 41.536, and the P value is less than 0.0001 (very significant level) ; the sum of squared errors within the group is 14.853, and the degree of freedom is 18. This indicates that different drying methods have a very significant effect on the uniformity of rice moisture content, and the difference between groups is much greater than the effect of random error within the group. The analysis results showed that the existence of the grain-turning device was a key factor in regulating the moisture uniformity of rice.

Table 3

ANOVA analysis of variance table

Variation source	Quadratic sum	Degree of freedom	Mean square	F statistic	The critical value a = 0.05	p-value	Significance
Between groups	3.9645	1	3.9645	41.536	4.41[$F_{0.05}(1,18)$]	< 0.001	very significant
Within the group	14.853	18	0.8252				
Grand total	18.8175	19					

CONCLUSIONS

1) Based on the thermal-fluid-solid coupling theory (THM), computational fluid dynamics (CFD) and particle discrete element method (DEM), two mathematical analytical models of cross-flow drying section with or without grain turnover device were established. The variation of drying rate and temperature rise of rice particles with drying time was revealed through experiments, and the reliability of the model was verified, which provided an important reference for the research of rice cross-flow drying equipment and the optimization of process parameters.

2) The EDEM-Fluent coupling method was used to simulate the drying process of rice, and the temperature and moisture content distribution of rice particles in the drying section were analyzed. The results show that the effect of the grain-turning device in the drying section is significant, which can promote the full mixing of rice particles and effectively improve the uneven distribution of temperature and humidity of rice particles.

3) Under strictly controlled operating conditions, comparative experiments were conducted on the drying process before and after the installation of an internal grain-turning device. The results of layered sampling and moisture content measurements showed that, prior to the improvement, the rice exhibited a pronounced moisture gradient within the drying section, reflecting the non-uniformity of heat and mass transfer processes. After the improvement, the moisture content distribution among different sampling layers became more uniform, and the interlayer differences were significantly reduced. Statistical validation using one-way analysis of variance further confirmed the effectiveness of the improved drying method. The results indicated an extremely significant difference between the two drying methods ($p < 0.001$), and at a significance level of 0.05, the F value was far greater than the critical value, demonstrating that the drying method had a decisive effect on moisture uniformity. These findings indicate that the grain-turning device enhances heat and mass transfer efficiency by regulating the relative positions of rice particles, thereby effectively alleviating localized over-drying or under-drying phenomena.

ACKNOWLEDGEMENT

This project is supported by the National Key Research and Development Program of China (2021YFD2100901).

REFERENCES

[1] Ariyaratne, W.K.H., Manjula, E.V.P.J., Ratnayake, C., Melaaen, M.C. (2016). CFD Approaches for Modeling Gas-Solids Multiphase Flows: A Review [C]. *Proceedings of the 9th EUROSIM Congress on Modelling and Simulation,* EUROSIM, pp.680-686, Vienna/Austria.

[2] Arsenoaia, V., Vlăduț, V., Țenu, I., Voicea, I., Cârlescu, P.M. (2019). Mathematical modeling and numerical simulation of the drying process of seeds in a pilot plant [J]. *INMATEH – Agricultural Engineering*, Vol.57, No.1, pp. 55-62, Bucharest/Romania.

[3] Cârlescu, P.M., Țenu, I., Roșca, R., Muscalu, A.T., Vlăduț, N.V. (2018). CFD simulation of an innovative vertical dryer for agricultural seeds drying, *PROCEEDINGS OF THE 46TH INTERNATIONAL SYMPOSIUM ON AGRICULTURAL ENGINEERING "Actual Tasks on Agricultural Engineering"*, pp. 407-418, Opatija/Croatia.

[4] Chen, G.X., Yue, L.F., Wang, Z.Q., Wang, H.T., Zhang, H. (2014). Numerical Simulation of Quasi-Static Temperature Field of Reinforced Concrete Underground Granary (钢筋混凝土地下粮仓准静态温度场数值模拟) [J]. *Chinese Journal of Cereals and Oils*, Vol.29, No.3, pp.79-82. Beijing/China.

[5] Duraisamy, K., Iaccarino, G., Xiao, H. (2019). Turbulence Modeling in the Age of Data [J]. *Annual Review of Fluid Mechanics*, Vol.51, pp.357-377. Palo Alto/USA.

[6] Hou, S.Q., Wang, Z.Y., Wang, W. (2018). Study on Shear Expansion Characteristics of Particles at Friction Interface Based on Hertz-Mindlin Contact Model (基于 Hertz-Mindlin 接触模型的摩擦界面颗粒剪切膨胀特性研究) [J]. *Journal of Hefei University of Technology (Natural Science Edition)*, Vol.41, No.12, pp.1601-1605. Hefei/China. (in Chinese with English abstract)

[7] Jia, F.G., Han, Y.L., Liu, Y., Cao, Y.P., Shi, Y.F., Yao, L.N., Wang, H. (2014). Simulation and Prediction Method of Accumulation Angle of Rice Particulate Matter (稻谷颗粒物料堆积角模拟预测方法) [J]. *Transactions of the Chinese Society of Agricultural Engineering (Transactions of the CSAE)*, Vol.30, No.11, pp.254-260. Beijing/China.

[8] Kjær, L.S., Poulsen, M., Sørensen, K., Condra, T. (2018). Modelling of Hot Air Chamber Designs of a Continuous Flow Grain Dryer [J]. *Engineering Science and Technology, an International Journal*, Vol. 21, No. 5, pp.1047-1051. Istanbul/Turkey.

[9] Li, C.Y., Mai, Z.W., Fang, Z.D. (2014). Analytical Method of Grain Moisture Binding Energy and Hot Air Drying Dynamics (粮食水分结合能与热风干燥动力解析法) [J]. *Transactions of the Chinese Society of Agricultural Engineering (Transactions of the CSAE)*, Vol.30, No.7, pp.236-240. Beijing/China.

[10] Li, C.Y., Ma, X.Z., Fang, Z.D., Zhang, Y. (2014). Thermal Energy Structure of Grain Hot Air Drying and Analytical Method (粮食热风干燥热能结构与解析法) [J]. *Transactions of the Chinese Society of Agricultural Engineering (Transactions of the CSAE)*, Vol.30, No.9, pp.220-228. Beijing/China.

[11] Li, X.G. (1998). Research and Computer Aided Design of Directional Ventilation Cross Flow Dryer (换向通风横流式干燥机的研究及计算机辅助设计) [J]. *Transactions of the Chinese Society of Agricultural Engineering (Transactions of the CSAE)*, Vol.14, No.2, pp.90-93. Beijing/China.

[12] Li, X.Z. (2023). Study on Heat and Mass Transfer Characteristics of Gas-Solid Coupling in Grain Particle Drying (谷物颗粒干燥气固耦合热质传递特性研究) [D]. *Hefei University of Technology*, Hefei/China, pp.9-14.

[13] Lv, J.H., Zhao, C.F., Li, J.C. (2010). Application and Analysis of Heat Pump Drying Technology in Agricultural and Sideline Products Processing (热泵干燥技术在农副产品加工中的应用与分析) [J]. *Agricultural Mechanization Research*, Vol.32, No.1, pp.212-217. Beijing/China.

[14] Padding, J.T., Deen, N.G., Peters, E.A.J.F., Kuipers, J.A.M. (2015). Euler-Lagrange Modeling of the Hydrodynamics of Dense Multiphase Flows [J]. *Advances in Chemical Engineering*, Vol.46, pp.137-191. San Diego/USA.

[15] Prakash, B., Siebenmorgen, T.J. (2018). Mathematical Modeling of a Cross-Flow Rice Dryer with Grain Inverters [J]. *Transactions of the American Society of Agricultural and Biological Engineers*, Vol.61, No.5, pp.1757-1765. St. Joseph/USA.

[16] Schluterman, G.J., Siebenmorgen, T.J. (2004). Air and Rice Property Profiles Within a Commercial Cross-Flow Rice Dryer [J]. *Applied Engineering in Agriculture*, Vol.20, No.4, pp.487-494. St. Joseph/USA.

[17] Sweet, J.N., Roth, E.P., Moss, M. (1987). Thermal Conductivity of Inconel 718 and 304 Stainless Steel [J]. *International Journal of Thermophysics,* Vol.8, No.5, pp.593-604. New York/USA.

[18] Wan, L., Wang, H.C., Che, G. (2019). Design and Experiment of Rice Hill-Direct-Seeding Device with Embedded Rotating Air Chamber (嵌入旋转气腔式水稻穴直播排种器设计与试验) [J]. *Transactions of the Chinese Society for Agricultural Machinery*, Vol.50, No.11, pp.74-84. Beijing/China.

[19] Wu, W.F., Liu, C.S., Han, F., Dai, L.Y., Li, J.X., Zhang, Y.Q. (2011). Current Situation and Trend of Grain Drying in China (中国粮食产地干燥的发展现状及趋势) [J]. *Transactions of the Chinese Society of Agricultural Engineering (Transactions of the CSAE)*, Vol.27, No.2, pp.321-324. Beijing/China.

[20] Wu, W.F., Zheng, X.Z., Ma, Z.S. (2001). Theory and Technology of Grain Drying and Storage (谷物干燥储藏理论与技术) [M]. *Jilin Science and Technology Press*, Jilin/China, pp.10-20.

[21] Xiao, S.W., Chen, S.Y., Liu, H.Y., Liu, C.S., Cui, B., Li, Z.A., Zhao, G.F. (2025). EDEM-Based Simulation Experiment on Drying Device Components (基于 EDEM 的干燥装置部件仿真试验研究) [J]. *Agricultural Mechanization Research*, Vol.47, No.6, pp.191-192. Beijing/China.

[22] Xu, Z.G., Zhang, Z.L., Liu, H.Y., Fu, N.Z., Bai, J.F., Cheng, S.K. (2020). Food-Away-from-Home Plate Waste in China: Preference for Variety and Quantity [J]. *Food Policy*, Vol.97, pp.1-7. Amsterdam/Netherlands.

[23] Yin, H.N., Yang, R.C., Miao, Q., Zhang, P.F., Bo, Zhao, H.Y., Qi, H., Zhang, K. (2025). Simulation and Optimization of Temperature Field of Crop Hot Air Oven Based on Numerical Simulation (基于数值模拟的农作物热风烘箱温度场模拟及优化) [J]. *China Agricultural Science and Technology Review*, pp.1-10. Beijing/China.

[24] Yang, Z., Luo, X.W., Li, C.Y. (2003). Experimental Determination of Thermal Parameters of Paddy (稻谷热特性参数的试验测定) [J]. *Transactions of the Chinese Society for Agricultural Machinery*, Vol.34, No.4, pp.77-78. Beijing/China.

[25] Zhang, M.Y., Luo, Y., Huang, M.M., Wu, L.P., Zhu, J.F. (2021). Maize Storage Losses and Its Main Determinants in China [J]. *China Agricultural Economic Review*, Vol.14, No.1, pp.17-31. Oxford/UK.